ARTICLE   OPEN

Increases in extreme precipitation over the Northeast United States using high-resolution climate model simulations

Bor-Ting Jong [1]✉, Thomas L. Delworth [2], William F. Cooke [2], Kai-Chih Tseng[1,3] and Hiroyuki Murakami [2,4]

Extreme precipitation is among the most destructive natural disasters. Simulating changes in regional extreme precipitation remains challenging, partially limited by climate models' horizontal resolution. Here, we use an ensemble of high-resolution global climate model simulations to study September–November extreme precipitation over the Northeastern United States, where extremes have increased rapidly since the mid-1990s. We show that a model with 25 km horizontal resolution simulates much more realistic extreme precipitation than comparable models with 50 or 100 km resolution, including frequency, amplitude, and temporal variability. The 25 km model simulated trends are quantitatively consistent with observed trends over recent decades. We use the same model for future projections. By the mid-21st century, the model projects unprecedented rainfall events over the region, driven by increasing anthropogenic radiative forcing and distinguishable from natural variability. Very extreme events (>150 mm/ day) may be six times more likely by 2100 than in the early 21st century.

INTRODUCTION

Extreme precipitation is expected to increase with global warming[1–5], which is a growing threat to the livelihoods of humans, and poses severe challenges for infrastructure planning. For example, the remnants of Hurricane Ida poured record-breaking rainfall in the Northeast United States (hereafter NEUS) on September 1, 2021, inundating the densely populated region including the New York City and Philadelphia metropolitan areas, causing at least 55 casualties and more than 20 billion dollars loss in the NEUS[6,7]. As the NEUS (see "Methods" and Supplementary Fig. 1) has faced the most rapidly increasing frequency of extreme precipitation within the United States in the past few decades[8–12], there has been rising concern about whether existing infrastructure is at risk of possible changes in a future warmer climate. Crucial information needed for planning includes how the frequency and amplitude of extreme events will change in the future, and whether/when future extreme events will be outside the currently observed record.

Detecting and projecting changes in extreme precipitation on regional scales, however, remain highly challenging and uncertain[3,13,14]. One of the primary limitations comes from models' coarse horizontal resolution[13,15]. Global climate models, commonly with atmospheric resolution ranging from 100 to 200 km (1–2°), are not sufficient to resolve the most extreme precipitation events and generally underestimate the rate of occurrence of the most extreme rates of precipitation[5,15–18]. Enhancing a model's horizontal resolution has been shown to improve the simulated frequency of extreme precipitation markedly, as higher precipitation rates are permitted by the higher-resolution model[15,16,18,19]. Also, models with finer resolutions better represent several physical processes related to extreme events such as tropical cyclones[15,18,20,21], extratropical transition[22], mesoscale processes[19,23], atmospheric rivers[24], and quasi-persistent weather regimes[25], compared to models with coarser resolutions.

Here, we use a high-resolution climate model, SPEAR (**S**eamless system for **P**rediction and **EA**rth system **R**esearch), developed at

National Oceanic and Atmospheric Administration (NOAA) Geophysical Fluid Dynamics Laboratory (GFDL)[26], to detect and project the increasing frequency of extreme precipitation over the NEUS. We focus on the boreal fall season (September to November), as the fall season has the most robust trend[27–29]. We first employ a variety of horizontal resolutions in the atmosphere/ land components of the model, ranging from 100 to 25 km, to demonstrate that a finer resolution model facilitates a more realistic simulation of extreme precipitation frequency than a coarser resolution model. We then investigate the observed and simulated past changes in extreme precipitation over the NEUS, as well as SPEAR-based projections of future changes in extreme precipitation. See "Methods" for more details about the model and observation dataset.

RESULTS

Resolution dependence of extreme precipitation simulations

To demonstrate that a model with higher horizontal resolution can simulate more realistic extreme precipitation frequency, we examine the probability density function (PDF) of the NEUS precipitation in the boreal fall season from the observations and SPEAR's three resolution configurations (Fig. 1 and Supplementary Fig. 2). For rainfall rates less than 10 mm/day, the model overestimates the frequency of occurrence. This is commonly known as the "excessive drizzle" issue in many climate models[15]. The model also underestimates the frequency of rainfall with 10–25 mm/day intensity and overestimates the frequency of rainfall with 25–40 mm/day intensity. Nevertheless, the performances of these three different configurations are consistent with each other. For extreme precipitation (99th percentile; indicated by vertical lines in Fig. 1; see "Methods" for defining the 99th percentile threshold), SPEAR_LO (100-km resolution) underestimates the frequency of precipitation intensity above the threshold and fails to simulate the most extreme observed events that are stronger than 150 mm/day. SPEAR_MED (50-km resolution) can

[1]Program in Atmospheric and Oceanic Sciences, Princeton University, Princeton, NJ, USA. [2]NOAA Geophysical Fluid Dynamical Laboratory, Princeton, NJ, USA. [3]Department of Atmospheric Sciences, National Taiwan University, Taipei, Taiwan, ROC. [4]University Corporation for Atmospheric Research, Boulder, CO, USA. ✉email: bor-ting.jong@noaa.gov

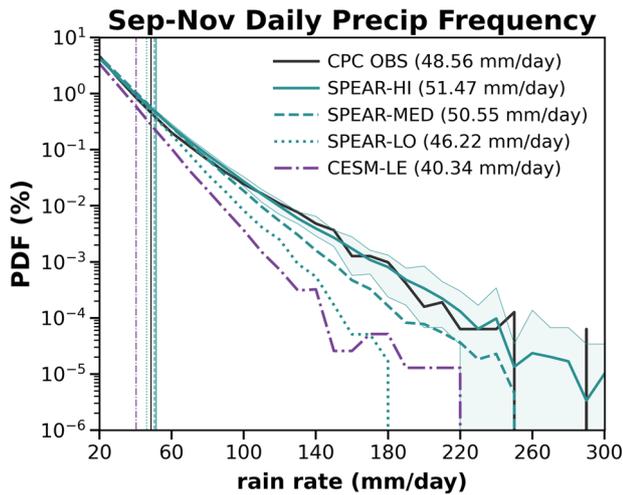## Sep-Nov Daily Precip Frequency

Fig. 1 Probability density function of daily precipitation over the NEUS in September to November during 1951–2020. The observation is shown by the black line. SPEAR_LO (100-km resolution), SPEAR_MED (50-km resolution), and SPEAR_HI (25-km resolution) simulations are shown in green dotted, dashed, and solid lines, respectively. CESM-LE (100-km resolution) is shown by the purple dash-dotted line. Only the spread of SPEAR_HI ensemble members is shown. The ensemble spreads for the other models are included in Supplementary Fig. 2. Vertical lines and the numbers shown in the legend indicate the thresholds of 99th percentile daily precipitation in each dataset or model (see "Methods" for the definition).

simulate a comparable frequency of extreme precipitation with the observations up to about 80 mm/day and then under-estimates the frequency of extremes above 80 mm/day. Only SPEAR_HI (25-km resolution) simulates extreme precipitation frequency comparable to the observations over the full range of extreme precipitation, even for the most extreme precipitation (such as 250 mm/day). These comparisons, consistent with previous studies[15,16], suggest that the frequency of very intense rainfall events such as Ida's remnants, which produced about 180 mm of rain in the New York City Central Park within one day[6,7], can only be reasonably simulated in the high-resolution configuration. The realistic simulation of precipitation frequency, including the full range of extreme precipitation, from SPEAR_HI therefore encourage us to use this version of the model to further study and project changes in extreme precipitation over the NEUS.

Trends of the NEUS extreme precipitation

The increasing occurrence of extreme precipitation over the NEUS has been robustly documented in many studies using station data and multiple extreme precipitation indices[10–12,27–37]. For example, the threshold for the top 1% of precipitation across all the NEUS stations for each year experienced a statistically significant 0.3 mm per year increasing trend with total increase of 10.8 mm from 1979 to 2014[29]. Similarly, the occurrence of precipitation events stronger than 150 mm/day increased from only six events between 1979 and 1996 to 25 events between 1997 and 2014[29]. The rising trend is also significant in the longer term: the total annual amount of precipitation falling in the top 1% events increased 58% from 1958 to 2016[11]. Most of the observed trend in annual extreme precipitation has occurred in the warm season[10,29,33]. Within the warm season, the fall season has the most robust trend[27–29]. Thus, we focus on the fall season in this model-based study.

In our results, the observed frequency of extreme precipitation, defined as the 99th percentile of daily accumulated precipitation (see "Methods"), over the NEUS in the fall season abruptly

increased in the mid-1990s, from ~0.5%/year in the early 1990s to ~1.5%/year in the late 2010s, after a relatively stable period in the 1980s (Fig. 2a and Supplementary Figs. 3 and 4). For the more recent period (1991–2020) the frequency of extreme events increased at a rate of 0.035% per year, while over the longer period (1951– 2020) the frequency increased at a rate of 0.011% per year. Both of these two trends are statistically significant at 95% confidence based on a *t* test. Consistent with previous studies, the increasing trend mostly happened since the late 1990s[28,29,34,35]. We also use three objective thresholds of 50 mm/day, 100 mm/day, and 150 mm/day, approximately corresponding to 99th, 99.9th, and 99.99th percentiles for the observations, respectively, to measure the variations of extreme precipitation (Fig. 2b–d)[29]. The breakdown clearly shows that very extreme precipitation (>150 mm/day) increased dramatically in the late 1990s: the likelihood of very extreme events was about 0.01% before the 1970s and less than 0.005% from the 1970s to the early 1990s. After the abruptly rising occurrence in the late 1990s, the frequency increased by a factor of three or more compared to earlier decades.

Compared to the observations, the ensemble mean of SPEAR_HI historical simulations produces realistic frequencies of extreme precipitation at all intensities. The simulations also show an increasing trend since the late 20th century (Fig. 2, green solid lines). The long-term increasing rate of the frequency of the 99th percentile events in the SPEAR_HI ensemble mean is 0.001% per year from 1951 to 2020, similar to the observations. The SPEAR_HI ensemble mean, however, does not simulate the abrupt increase in extreme precipitation since the mid-1990s shown in the observations. The frequency in the SPEAR_HI ensemble mean gradually increases from the early 1980s at a rate of ~+0.011% per year from 1991 to 2020, much slower than the observed rate (but statistically significant at 95% confidence based on a *t* test). As the ensemble mean of SPEAR_HI represents the responses to the external radiative forcing, the more gradual trend and smaller variations suggest that natural climate variability contributed substantially to the historical variability of extreme precipitation over the NEUS[38]. We therefore employ ensembles to better constrain the internal variability in extreme precipitation. The shaded envelopes in Fig. 2 indicate the spread of the 10 ensemble members in the SPEAR_HI simulations. SPEAR_HI ensemble members do present larger interannual to multidecadal variability, but the spread does not contain the observations during the period around 1990 when extreme events were less common and the period around 2011 when extreme events occurred more frequently (Fig. 2a). One plausible reason is that 10 ensemble members are not sufficient to capture the full range of possible variations associated with the internal variability in extreme precipitation.

To complement the limited ensemble size in SPEAR_HI, we next examine the 30-member simulations from SPEAR_MED and SPEAR_LO (see "Methods"). SPEAR_MED and SPEAR_LO under-estimate the extreme precipitation characterized by absolute values (Fig. 2b–d), especially for the 100-km configuration which marginally permits very extreme precipitation (Fig. 2c, d, dotted green lines). The ensemble means of SPEAR_MED and SPEAR_LO, nevertheless, simulate the variations and trends of the extreme precipitation defined by the 99th percentile threshold similar to the ones simulated by SPEAR_HI (Fig. 2a). The larger size of the ensemble from SPEAR_MED and SPEAR_LO displays a larger spread of internal variability and encompasses most of the observed temporal variability of extreme precipitation over the NEUS, except the peak period around 2011 (Supplementary Figs. 5 and 6). This suggests that if we increased the number of ensembles for SPEAR_HI, it would show reasonable ensemble spread as SPEAR_MED does. The 40-member CESM-LE simulations with 100-km resolution present similar results: the ensemble mean of CESM-LE 99th percentile events shows a slightly increasing
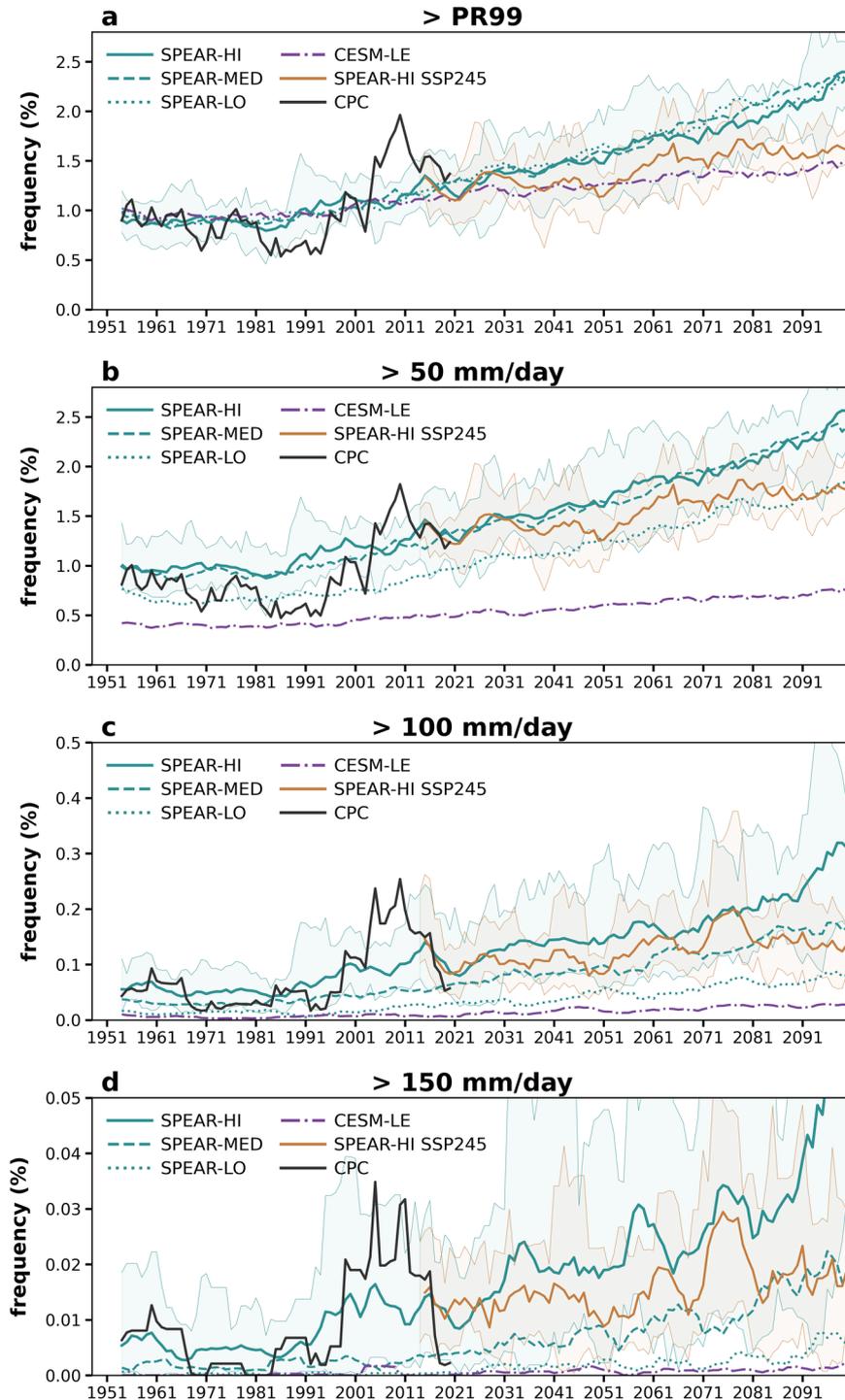
Fig. 2 Time series showing the changes in the frequency of extreme precipitation in each year from 1951–2100. a Extreme events are defined as exceeding the 99th percentile threshold based upon 1951–2020 from each dataset or model (see "Methods"). **b–d** As in (**a**), but extreme events are defined as exceeding thresholds of 50 mm/day, 100 mm/day, and 150 mm/day. The observation is shown in black lines. The ensemble mean of SPEAR_LO, SPEAR_MED, and SPEAR_HI historical and SSP5-8.5 simulations are shown in green dotted, dashed, and solid lines, respectively. The SPEAR_HI SSP2-4.5 simulations for 2015–2100 are also included (orange solid lines). The ensemble mean of CESM-LE historical and RCP5.8 simulations is presented by purple dash-dotted lines. Only the spreads of SPEAR_HI ensemble members are shown. The ensemble spreads for the other models are included in Supplementary Figs. 5–7. The time series are smoothed with a 7-year running mean to remove the interannual variability, emphasizing the long-term trend and variability.
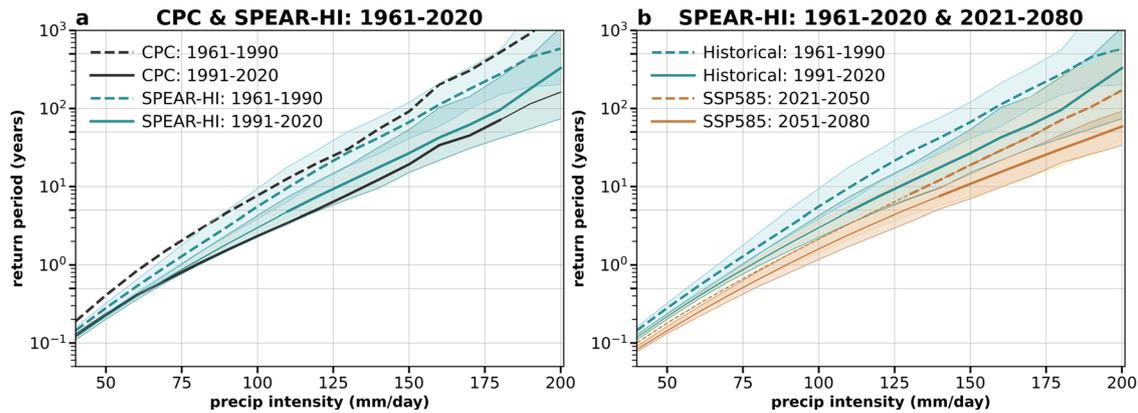
Fig. 3 Return periods of extreme precipitation events using different thresholds as seen in the observations and SPEAR_HI. a Compare the return periods in 1961–1990 (dashed lines) and 1991–2020 (solid lines). The observations and SPEAR_HI ensemble mean are shown in black and green lines, respectively. **b** Compare the return periods in the SPEAR_HI historical (green lines) and SSP5-8.5 (orange lines) simulations between 2021 and 2080 versus 1961 and 2020. Shaded area encompasses the spread of the SPEAR_HI ensemble. Thick solid lines indicate the changes compared with the earlier 30-year period are statistically significant at 95% confidence interval using the bootstrapping method. The y-coordinate is shown in a logarithmic scale and is in the unit of years.

trend since the 1990s (Fig. 2a, purple line). The ensemble spread covers most of the observed variability except the peak around 2011 (Supplementary Fig. 7). The model, however, considerably underestimates the frequency of extreme precipitation characterized by absolute values (Fig. 2b–d) partially due to its coarser resolution.

Detecting change in the probability of extreme precipitation

The elevated frequency of NEUS extreme precipitation in the last three decades can also be demonstrated by the change in the probability of extreme events with different intensities. Here, we compare the return period of extreme precipitation for the entire NEUS region during 1961–1990 versus 1991–2020 (Fig. 3a; see "Methods" for the calculation of return period). In the observations, an event with 50 mm/day or greater intensity had a 0.4-year return period in 1961–1990, meaning that such an event would occur on average over 0.4 years (equivalent to 150 days) somewhere in the NEUS region. The return period of a 50 mm/day event, however, had become 0.23 years in the past three decades, nearly doubling the probability. For an event with 180 mm/day intensity, corresponding to the daily rainfall measured in New York City caused by Hurricane Ida's remnants,[6,7] the return period had dropped from 520 years in 1961–1990 to 70 years in 1991–2020, almost seven times more likely in the latter period.

In the ensemble mean of SPEAR_HI, the simulated return period for a 50 mm/day (or stronger) event is about 0.3 years in 1961–1990 and 0.22 years in 1991–2020, but the change during these two periods is statistically insignificant at the 95% confidence interval. For an event with 180 mm/day intensity, the simulated change in the return period significantly declines from 270 years in 1961–1990 to 95 years in 1991–2020. While the ensemble mean of SPEAR_HI simulates a higher rate of frequency of extreme precipitation during 1961–1990 compared to the observations, and a lower rate compared to the observations for 1991–2020, the observed probability in both periods is mostly within the spread of the ensemble members. This suggests that the dramatic increase in the frequency of extreme precipitation since the 1990s in observations has been driven by both external radiative forcing and natural climate variability.

Projecting future extreme precipitation frequency

Extreme precipitation in the NEUS is expected to become more frequent due to anthropogenic warming[5,30,39–42]. To project future

changes in the NEUS extreme precipitation, SPEAR_HI, which has shown high performance in simulating the frequency and variability of extreme precipitation in the present climate, is useful to evaluate how intense and frequent the extreme events will be. In addition, will we see any unprecedented events in the near future (extreme events larger than any yet observed)?

Using the 99th percentile threshold based on 1951–2020 climatology, the ensemble mean of SPEAR_HI projects the frequency of extreme precipitation would become 2.4% per year by the end of the 21st century under the SSP5-8.5 high-emissions scenario, which doubles the frequency compared to the current value (Fig. 2a). In the SSP2-4.5 scenario, considered by some as a more realistic emission trajectory[43], the frequency would become 1.6% per year by 2100. The increasing rate, however, is not uniform for all intensities among the extreme precipitation range, as the tails of the probability distribution may experience more dramatic change[13]. For instance, the frequency of events exceeding 100 mm/day would triple, from about 0.1% in the recent three decades to 0.3% in 2100, under the SSP5-8.5 (Fig. 2c); while the frequency of events exceeding 150 mm/day would become six times more frequent compared to the recent three decades (~0.01%) by the end of the 21st century (~0.06%; Fig. 2d). The frequency, on the other hand, would increase less rapidly under the SSP2-4.5 scenario: the frequency of event exceeding 100 mm/day would increase to about 0.15%; while the frequency of event exceeding 150 mm/day would increase to about 0.02% by 2100 (orange lines in Fig. 2c, d).

The projected changes in return period for different event intensities also demonstrate that the likelihood of more intense extreme events would increase more rapidly (Fig. 3b). For example, an event with 50 mm/day intensity or stronger is currently a 1-in-0.22-year event in the NEUS region in the SPEAR_HI ensemble mean, meaning that such an event would occur on average over 0.22 years (that is, 80 days) somewhere in the NEUS region. This kind of event would become a 1-in-0.18 year event by 2050 and an approximate 1-in-0.14-year event by 2100 under the SSP5-8.5 scenario. On the other hand, a very extreme event with 200 mm/day intensity would change from a 1-in-330-year event to a 1-in-170-year event by 2050 and a 1-in-58-year event by 2100. This dramatic projected increase in the probability is statistically significant at 95% confidence interval based on a bootstrapping resampling method.

While extreme precipitation is projected to be more frequent and intense, we would not necessarily see more unprecedented events by the mid-21st century given the large internal variability.
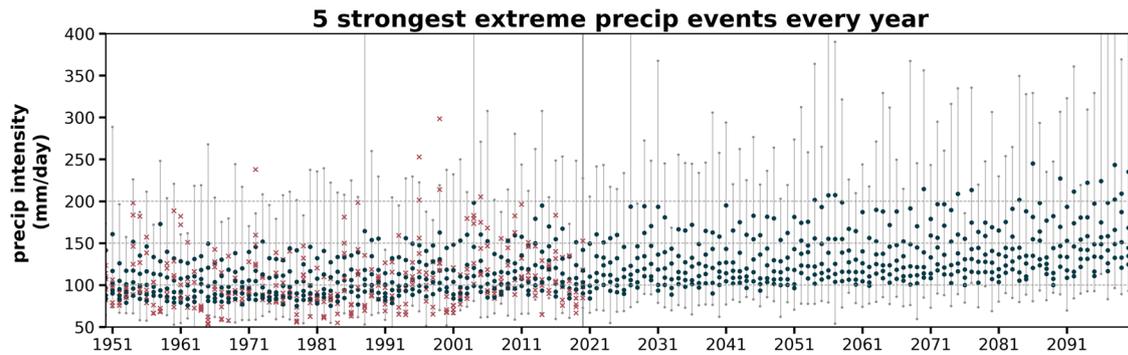
5 strongest extreme precip events every year

Fig. 4 Five strongest extreme precipitation events in the NEUS autumn from 1951 to 2100. Blue color dots are the intensity of the annual five strongest events in the ensemble mean of SPEAR_HI historical (1951–2014) and SSP5-8.5 (2015–2100) simulations. Thin gray lines indicate the ensemble spread of the five strongest events in each ensemble member each year. Pink crosses are the intensity of the annual five strongest events from the observations. The vertical black line indicates the year of 2020. The time series is not smoothed with a 7-year running mean as in Fig. 2, since the context is to emphasize the strong internal variability of extreme precipitation.
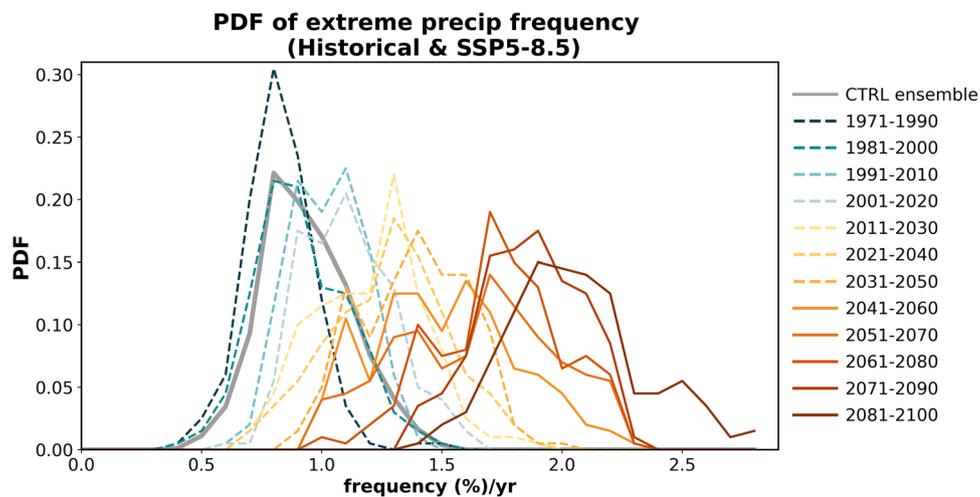
PDF of extreme precip frequency
(Historical & SSP5-8.5)

Fig. 5 Change in the distribution of extreme precipitation frequency. Each color line presents the probability density function of extreme precipitation frequency each year in a 20-year period from the SPEAR_HI historical (cold colors) and SSP5-8.5 (warm colors) simulations. The thick gray line is the PDF of extreme precipitation frequency from the preindustrial control simulations. Solid (dashed) lines indicate the medians of the distributions from the historical or SSP5-8.5 simulations are (not) statistically significantly different from the median of the distribution based on the control simulations at 95% confidence interval. See "Methods" for the details.

Figure 4 shows the intensity of the five strongest events in each autumn from individual ensemble members (gray lines show the spread) and ensemble mean (blue color dots) in the SPEAR_HI historical and SSP5-8.5 simulations from 1951 to 2100. In the observations, the recorded high event happened in 1999 with 298 mm/day intensity. The ensemble spread of SPEAR_HI does not frequently encompass this record until the mid-21st century. However, as indicated above, 10 ensemble members from SPEAR_HI may not be sufficient to cover the full range of internal variability, so the timing when unprecedented events will emerge might be earlier than the estimation. In the ensemble mean, the five strongest events in each year range between 80 to 200 mm/day in intensity in the historical period. The range would become 100 to 200 mm/day in the mid-21st century. While unprecedented events would probably not arise until the mid-21st century, the lower bound for defining the annual five strongest events, in both the ensemble spread and mean, has increased since the 1990s, consistent with previous results that extreme precipitation has increased and become more intense[10–12,27–34,36]. The more frequent extreme event means the time interval between two consecutive extreme events would become shorter, enhancing threats of flooding. For instance, in 2021, Tropical cyclone Henri brought a 100-year rainstorm to the NEUS just two weeks before

the remnants of Hurricane Ida swept through the region. The extreme rainfall brought by Henri saturated the ground, which was one of the major reasons that Ida's remnants could cause such severe flash floods across the NEUS[7].

Estimating the time of signal emergence
The increasing trend of the NEUS extreme precipitation may be attributed to both anthropogenic forcing and internal variability. The signal of the forced increase in the extreme precipitation frequency, however, will eventually emerge from the noise of internal variability[44–47]. To estimate this "time of emergence" for the frequency of NEUS extreme precipitation, we calculate when the shift in the median values of extreme precipitation frequency per year from the SPEAR_HI historical and SSP5-8.5 simulations becomes statistically significant, compared to the median values from the preindustrial control simulation (see "Methods"; Fig. 5). Under the SSP5-8.5 scenario, the shift in the median value of the frequency first becomes statistically significantly different from the median value based on the control simulation in the mid-21 century (2041–2060), at 95% confidence interval, and the significant shift remains thereafter. That means, if the SSP5-8.5 scenario of emissions is followed, the contribution of

anthropogenic forcing to the increasing trend of the NEUS extreme precipitation would become distinguishable from the contribution of random internal variability in 20–30 years. If the SSP2-4.5 is followed, the time of emergence for the NEUS extreme precipitation frequency could be delayed for 10–20 years (by 2051–2070), compared with the one under the SSP5-8.5 scenario (Supplementary Fig. 8).

DISCUSSION

Projecting future changes in regional extreme precipitation is a vital need but presents significant challenges. Simulations of the regional characteristics of extreme precipitation can often be improved in climate models with higher horizontal resolution, as higher resolution can better resolve extreme precipitation events. Hence, an ensemble of climate simulations using high-resolution coupled models provides a valuable tool for evaluating projected changes in extreme precipitation characteristics and can benefit infrastructure design and resilience planning. One caveat of our study is that we only evaluate the simulations for the NEUS region from SPEAR models and CESM-LE. The results that higher horizontal resolution simulates better extreme precipitation features in the NEUS should be further assessed for other regions and other climate models[48,49].

While high resolution can advance more realistic simulations of extreme precipitation statistics, we show that large ensembles are also critical to estimating future changes in the most extreme precipitation events. In the ensemble mean of SPEAR_HI, the frequency of events with an intensity of 50 mm/day or even 100 mm/day steadily increases in the 21st century in response to increasing radiative forcing (Fig. 2b, c, green solid lines). In contrast, events with an intensity of 150 mm/day or larger increase at a more irregular rate (Fig. 2d, green solid line), suggesting that the ensemble size used (10 members for the highest resolution simulations with the strongest radiative forcing changes, SSP5-8.5) may not be sufficient to robustly sample the most extreme events. In the more moderate radiative forcing scenario used (SSP2-4.5), only six ensemble members are available in SPEAR_HI. As a result, the six-member ensemble mean is substantially impacted by natural variability contained in the individual ensemble members, such that there are extended periods when the ensemble mean has little discernible trend and large multidecadal variability (Fig. 2, orange lines). These results point to the need for very large ensembles to robustly quantify changes in extreme precipitation, especially for the most extreme events, simulated in climate models.

Despite the uncertainty associated with limited ensembles, our results show that an increase in the likelihood of extreme precipitation in the NEUS during September–November is a robust finding since SPEAR_HI simulates the long-term variability of extreme precipitation consistent with previous studies and the observations are mostly within the spread of the ensemble. Ongoing work focuses on process-based assessments including how various types of precipitation events, such as tropical cyclones, extratropical transition, atmospheric rivers, or convective storms, contribute to the extreme precipitation trend in both observations and SPEAR_HI[34,37,40,50,51]. Also, further assessment of how SPEAR_HI simulates extreme precipitation in other regions and seasons will provide additional insight into the advantages and limitations of high-resolution climate models.

METHODS

Northeast US region

In this study, the Northeast US (NEUS) region is defined as the US land territory within 37–50°N, 80.5–67°W, encompassing the states of Maine, New Hampshire, Vermont, Massachusetts, Rhode Island, Connecticut, New York, New Jersey, Pennsylvania, Delaware, Maryland, Washington D.C., and parts of Virginia and West Virginia. See Supplementary Fig. 1 for the location of the NEUS region.

Observational data

In this study, we use gridded daily precipitation data from NOAA Climate Prediction Center (CPC) Unified Gauge-Based Analysis[52] with resolution at 0.25° by 0.25° for the period of 1948 to 2020. We choose this dataset because (1) it provides a longer period of record for assessing long-term variations and trends in extreme precipitation; (2) this gridded dataset has a relatively fine horizontal resolution that is comparable to SPEAR_HI; and (3) previous studies have suggested that this dataset has a remarkable quality and small bias over the continental US[53] and has been chosen to assess the US extreme precipitation in historical simulations from the Coupled Model Intercomparison Project 6 (CMIP6) models[54]. While most of the previous studies focusing on the NEUS extreme precipitation used station data such as Global Historical Climatology Network daily[33,34,37,55], the CPC-gridded data shows the consistent temporal variations is extreme precipitation frequency for the period of 1948–2020 (Supplementary Fig. 3).

Models

We use daily precipitation output from two modeling systems. The first is called SPEAR (**S**eamless system for **P**rediction and **EA**rth system **R**esearch)[26]. SPEAR is NOAA (National Oceanic and Atmospheric Administration) GFDL (Geophysics Fluid Dynamics Laboratory)'s latest coupled GCM, building from GFDL's most recently developed atmospheric (AM4), land (LM4)[56,57], oceanic (MOM6), and sea-ice (SIS2)[58] component models. SPEAR uses similar component models as GFDL Global Climate Model version 4 (CM4)[59] and Earth System Model 4 (ESM4)[60] which participated in the CMIP6. The configuration of SPEAR is optimized for the study of seasonal to multidecadal variability, predictability, and projection.

SPEAR provides different options for atmospheric horizontal resolution, ranging from 1 to 0.25°. Here, we mainly use a high-resolution configuration, SPEAR_HI, with 0.25° grid spacing in the atmosphere and land components to better simulate extreme precipitation. We also use the simulations from low-resolution (SPEAR_LO, 1° atmosphere/land) and medium-resolution (SPEAR_MED, 0.5° atmosphere/land) configurations to assess the resolution dependence of the simulations of extreme precipitation. The physics are identical across these three configurations, with the exception of modest tuning in the damping and advection parameters for SPEAR_HI to improve the simulation of tropical storms. The model timesteps change with resolution for numerical stability. All configurations are coupled to the same 1° ocean model (with tropical refinement to 0.3°). The details of SPEAR's physical parameterizations and configurations can be found in ref. [26].

All historical simulations are driven by the observed time-evolving changes in radiative forcing agents (greenhouse gases, aerosols, land use, solar irradiance, and volcanic aerosols) over the period of 1921 to 2014. From 2015 to 2100 the models are forced by projected changes in radiative forcing agents, using either Shared Socioeconomic Pathway 5-8.5 (SSP5-8.5) or 2-4.5 (SSP2-4.5)[61,62]. Since the SSP5-8.5 represents a very high-end projection of future anthropogenic radiative forcing changes, and is sometimes considered an overestimate of projected future warming[43], it is important to include simulations with the "middle of the road" SSP2-4.5 scenario for comparison. SPEAR_LO and SPEAR_MED both have 30 ensemble members for the historical and SSP5-8.5 simulations; while SPEAR_HI has 10 ensemble members for the historical and SSP5-8.5 simulations and six ensemble members for

the SSP2-4.5 simulations. Each ensemble member is initialized from a different year from their respective long control simulations with 20-year spacing to sample different phases of internal variability. These perturbations applied to the initial conditions of ensemble members create diverging weather and climate trajectories and thereby ensemble spread, which represents natural climate variability. These unpredictable and random internal variability is presumably canceled out in the ensemble mean, so the ensemble mean can be estimated as responses to external radiative forcing[38].

A 1000-year preindustrial control simulation from SPEAR_HI is also used to represent internal natural variability. In the control simulation, radiative forcing and land-use conditions are fixed at levels of the year 1850 to represent preindustrial conditions. We analyze the last 900 years in the simulations.

CESM-LE

We also examine daily precipitation from the Large Ensemble of Community Earth System Model version 1 (termed as CESM-LE in this study) which has 40 members performed at a 1° horizontal resolution[63]. CESM-LE includes historical simulations driven by historical time-evolving radiative forcing from 1920 to 2005 and the "high-emissions" Representative Concentration Pathway 8.5 (RCP8.5) simulations from 2005 to 2100. Each ensemble member of CESM-LE is driven by the same forcing but initialized with slightly different initial conditions in the temperature field which is randomly perturbed at the level of round-off error.

To be consistent with the observation, we only use the output since the year 1948 from the historical simulations of both SPEAR and CESM-LE.

Definition of extreme precipitation

We define extreme precipitation as daily accumulated precipitation falling in the 99th percentile (top 1%) of recorded wet days (≥0.1 mm/day) from September to November. The 99th percentile threshold of daily precipitation is consistently determined based on the years 1951 to 2020 for both the observations and the models. For the observations, all the grid points within the NEUS region are aggregated to derive the threshold. For SPEAR and CESM-LE, all the ensemble members and grid points within the NEUS region in each model are included to calculate the 99th percentile threshold for the corresponding model.

We choose this method rather than using spatially varied thresholds for two reasons: (1) We also define a 99th percentile threshold of recorded wet days at each grid point individually (Supplementary Fig. 1), and then count the number of occurrences for each year at each grid point, averaging across the NEUS region (Supplementary Fig. 4). The area-averaged frequency variations using the spatially varied threshold are very similar to the frequency variations using the constant 99th percentile threshold (compared Supplementary Fig. 4 with Fig. 2a); (2) In our analyses, we also use objective thresholds, 50 mm/day, 100 mm/day, and 150 mm/day, to emphasize the advantage of the high-resolution model in simulating very extreme precipitation (Fig. 2b–d). For fair comparisons, the constant 99th percentile threshold across the region is thereby used in this study.

Return period

Return period, also called recurrence interval[64], measures the average time interval between the occurrence of events such as extreme precipitation. Theoretically, return period is the inverse of the frequency of occurrence, so it also represents probability of occurrence. For example, the return period for the 99th percentile (top 1%) daily precipitation event is about 0.3 years (that is, there is a 1% chance that a daily precipitation event has equal or

stronger intensity than the 99th percentile threshold in any 100 days or 0.3 years)[65].

In this study, return period for an event with X mm/day or stronger intensity is calculated as,

$$return\,period(X) = \frac{N + 1}{R} \qquad (1)$$

N is the number of total recorded rainy days (≥0.1 mm/day) in September to November in the specified year range. R is the rank of X mm/day among all the rainy days in descending order. Same as the selection of the 99th percentile thresholds: for the observations, all the grid points within the NEUS region are aggregated (to increase the sample sizes). For SPEAR_HI, all the ensemble members and grid points within the NEUS region in each model are included. Thus, the return period calculated here (Fig. 3) is for the NEUS as a whole, rather than for each grid point. That is, a 1-in-0.3-year event means there is a 1% chance that a daily precipitation event has equal or stronger intensity than the 99th percentile threshold in any 0.3 years (or 100 days) somewhere within the NEUS region.

To test whether the changes in the return periods for two consecutive 30-year periods are significantly different, bootstrapping resampling is conducted. We randomly select two 30-year periods with different start dates within the 60-year periods (so the two selected 30-year periods may partially overlap) in either the observations or SPEAR_HI and calculate the differences in the return periods of these two 30-year periods. We then repeat the procedure 500 times to approximate the distribution of the sample mean and assess the significance of the targeted differences.

Time of emergence

Time of emergence estimates the timing when an anthropogenic forced signal in climate extreme would emerge from the noise of atmospheric internal variability[44–46]. To estimate the time of emergence of extreme precipitation frequency over the NEUS, we compare the distributions of extreme precipitation frequency per year from SPEAR_HI historical and SSP5-8.5 simulations with the distribution from SPEAR_HI preindustrial control simulations which possess only internal natural variability. Time of emergence is therefore when the distributions in the historical or SSP5-8.5 simulations are significantly shifted from the distribution based on the control simulation.

In the control simulations, from the 900-year time series of extreme precipitation frequency, we randomly chunk a hundred 20-year periods to estimate the ensemble spread, mimicking the range of internal variability in extreme precipitation frequency. Extreme precipitation here is defined by the 99th percentile threshold based on the entire 900 years. Extreme precipitation in the historical and SSP5-8.5 simulations is defined by the 99th percentile threshold based on 1951–2020.

To analyze the shift in the distributions, the differences in the median of extreme precipitation frequency for each 20-year from the historical and SSP5-8.5 simulations and the median from the control simulation are calculated[46]. The statistical significance of differences in the median is assessed using bootstrapping resampling. We randomly selected two 20-year periods from the historical and SSP5-8.5 simulations within 1951 to 2100 and calculate the difference in the median of extreme precipitation frequency during these two 20-year periods. The procedure is repeated 500 times to evaluate the significance of the targeted differences.

REFERENCES
1. Allen, M. R. & Ingram, W. J. Constraints on future changes in climate and the hydrologic cycle. *Nature* **419**, 228–232 (2002).
2. Fischer, E. M., Beyerle, U. & Knutti, R. Robust spatially aggregated projections of climate extremes. *Nat. Clim. Change* **3**, 1033–1038 (2013).
3. Kharin, V. V., Zwiers, F. W., Zhang, X. & Wehner, M. Changes in temperature and precipitation extremes in the CMIP5 ensemble. *Clim. Change* **119**, 345–357 (2013).
4. O'Gorman, P. A. & Schneider, T. The physical basis for increases in precipitation extremes in simulations of 21st-century climate change. *Proc. Natl Acad. Sci. USA* **106**, 14773–14777 (2009).
5. O'Gorman, P. A. Precipitation extremes under climate change. *Curr. Clim. Change Rep.* **1**, 49–59 (2015).
6. Beven, J. L. II, Hagen, A. & Berg, R. National Hurricane Center Tropical Cyclone Report: Hurricane Ida. https://www.nhc.noaa.gov/data/tcr/AL092021_Ida.pdf (2022).
7. National Centers for Environmental Information. State of the climate: Monthly National Climate Report for Annual 2021. https://www.ncei.noaa.gov/access/monitoring/monthly-report/national/202113 (2022).
8. Kunkel, K. E. et al. Monitoring and understanding trends in extreme storms: State of knowledge. *Bull. Am. Meteorol. Soc.* **94**(4), 499–514 (2013).
9. Janssen, E., Wuebbles, D. J., Kunkel, K. E., Olsen, S. C. & Goodman, A. Observational- and model-based trends and projections of extreme precipitation over the contiguous United States. *Earth's Future* **2**, 99–113 (2014).
10. Hoerling, M. et al. Characterizing recent trends in U.S. heavy precipitation. *J. Clim.* **29**, 2313–2332 (2016).
11. Easterling, D. R. et al. Precipitation change in the United States. in *Climate Science Special Report: Fourth National Climate Assessment* (eds. Wuebbles, D. J. et al.) Vol. 1, 207–230 (U.S. Global Change Research Program, 2017).
12. DeGaetano, A. T., Moores, G. & Favata, T. Temporal changes in the areal coverage of daily extreme precipitation in the Northeastern United States using high-resolution gridded data. *J. Clim.* **59**, 551–565 (2020).
13. Xie, S.-P. et al. Towards predictive understanding of regional climate change. *Nat. Clim. Change* **5**, 921–930 (2015).
14. Pfahl, S., O'Gorman, P. A. & Fischer, E. M. Understanding the regional pattern of projected future changes in extreme precipitation. *Nat. Clim. Change* **7**, 423–427 (2017).
15. Wehner, M. F. et al. The effect of horizontal resolution on simulation quality in the Community Atmospheric Model, CAM 5.1. *J. Adv. Model Earth Syst.* **6**, 980–997 (2014).
16. Wehner, M. F., Smith, R. L., Bala, G. & Duffy, P. The effect of horizontal resolution on simulation of very extreme US precipitation events in a global atmosphere model. *Clim. Dyn.* **34**, 241–247 (2010).
17. Bador, M. et al. Impact of higher spatial atmospheric resolution on precipitation extremes over land in global climate models. *J. Geophys. Res. Atmos.* **125**, e2019JD032184 (2020).
18. Van der Wiel, K. et al. The resolution dependence of contiguous U.S. precipitation extremes in response to CO_2 forcing. *J. Clim.* **29**, 7991–8012 (2016).
19. Lucas-Picher, P., Laprise, R. & Winger, K. Evidence of added value in North American regional climate model hindcast simulations using ever-increasing horizontal resolutions. *Clim. Dyn.* **48**, 2611–2633 (2017).
20. Murakami, H. et al. Simulation and Prediction of category 4 and 5 hurricanes in the high-resolution GFDL HiFLOR coupled climate model. *J. Clim.* **28**, 9058–9079 (2015).
21. Roberts, M. J. et al. Impact of model resolution on tropical cyclone simulation using the HighResMIP–PRIMAVERA multimodel ensemble. *J. Clim.* **33**, 2557–2583 (2020).
22. Baker, A. J. et al. Extratropical transition of tropical cyclones in a multiresolution ensemble of atmosphere-only and fully coupled global climate models. *J. Clim.* **35**, 5283–5306 (2022).
23. Dong, W., Zhao, M., Ming, Y. & Ramaswamy, V. Representation of tropical mesoscale convective systems in a general circulation model: climatology and response to global warming. *J. Clim.* **34**, 5657–5671 (2021).
24. Zhao, M. Simulations of atmospheric rivers, their variability, and response to global warming using GFDL's new high-resolution general circulation model. *J. Clim.* **33**, 10287–10303 (2020).
25. Dawson, A. & Palmer, T. N. Simulating weather regimes: impact of model resolution and stochastic parameterization. *Clim. Dyn.* **44**, 2177–2193 (2015).
26. Delworth, T. L. et al. SPEAR: the next generation GFDL modeling system for seasonal to multidecadal prediction and projection. *J. Adv. Model. Earth Syst.* **12**, e2019MS00189 (2020).
27. Kunkel, K. E. et al. Regional climate trends and scenarios for the U.S. National Climate Assessment. Part 1. Climate of the Northeast U.S. https://scenarios.globalchange.gov/sites/default/files/NOAA_NESDIS_Tech_Report_142-1-Climate_of_the_Northeast_U.S_1.pdf (2013).
28. Huang, H., Winter, J. M., Osterberg, E. C., Horton, R. M. & Beckage, B. Total and extreme precipitation changes over the Northeastern United States. *J. Hydrometeorol.* **18**, 1783–1798 (2017).
29. Howarth, M. E., Thorncroft, C. D. & Bosart, L. F. Changes in extreme precipitation in the Northeast United States: 1979–2014. *J. Hydrometeorol.* **20**, 673–689 (2019).
30. Hayhoe, K. et al. Past and future changes in climate and hydrological indicators in the US Northeast. *Clim. Dyn.* **28**, 381–407 (2007).
31. Brown, P. J., Bradley, R. S. & Keimig, F. T. Changes in extreme climate indices for the Northeastern United States, 1870–2005. *J. Clim.* **23**, 6555–6572 (2010).
32. Agel, L. et al. Climatology of daily precipitation and extreme precipitation events in the Northeast United States. *J. Hydrometeorol.* **16**, 2537–2557 (2015).
33. Frei, A., Kunkel, K. E. & Matonse, A. The seasonal nature of extreme hydrological events in the Northeastern United States. *J. Hydrometeorol.* **16**, 2065–2085 (2015).
34. Huang, H., Winter, J. M. & Osterberg, E. C. Mechanisms of abrupt extreme precipitation change over the Northeastern United States. *J. Geophys. Res. Atmos.* **123**, 7179–7192 (2018).
35. Huang, H., Patricola, C. M., Winter, J. M., Osterberg, E. C. & Mankin, J. S. Rise in Northeast US extreme precipitation caused by Atlantic variability and climate change. *Weather Clim. Extrem.* **33**, 100351 (2021).
36. Olafsdottir, H. K., Rootzen, H. & Bolin, D. Extreme rainfall events in the Northeastern United States become more frequent with rising temperatures, but their intensity distribution remains stable. *J. Clim.* **34**, 8863–8877 (2021).
37. Henny, L., Thorncroft, C. D. & Bosart, L. F. Changes in large-scale fall extreme precipitation in the Mid-Atlantic and Northeast United States, 1979–2019. *J. Clim.* **35**, 3047–3070 (2022).
38. Deser, C. et al. Insights from Earth system model initial-condition large ensembles and future prospects. *Nat. Clim. Change* **10**, 277–286 (2020).
39. Ning, L., Riddle, E. E. & Bradley, R. S. Projected changes in climate extremes over the Northeastern United States. *J. Clim.* **28**, 3289–3310 (2015).
40. Zhao, M. A study of AR-, TS-, and MCS-associated precipitation and extreme precipitation in present and warmer climates. *J. Clim.* **35**, 479–497 (2022).
41. DeGaetano, A. Projected changes in extreme rainfall in New Jersey based on an ensemble of downscaled climate model projections. https://www.nj.gov/dep/dsr/publications/projected-changes-rainfall-model.pdf (2021).
42. Nazarian, R. H., Vizzard, J. V., Agostino, C. P. & Lutsko, N. J. Projected changes in future extreme precipitation over the Northeast US in the NA-CORDEX ensemble. *J. Appl. Meteorol. Clim.* **61**, 1649–1668 (2022).
43. Hausfather, Z. & Peters, G. P. Emissions—the 'business as usual' story is misleading. *Nature* **577**, 618–620 (2020).
44. Hawkins, E. & Sutton, R. Time of emergence of climate signals. *Geophys. Res. Lett.* **39**, L01702 (2012).
45. King, A. D. et al. The timing of anthropogenic emergence in simulated climate extremes. *Environ. Res Lett.* **10**, 094015 (2015).
46. King, A. D., Donat, M. G., Hawkins, E. & Karoly, D. J. Timing of anthropogenic emergence in climate extremes. in *Climate Extremes: Patterns and Mechanisms* (eds Wang, S.-Y.S. et al.) 93–103 (American Geophysical Union, 2017).
47. Zhang, H. & Delworth, T. L. Robustness of anthropogenically forced decadal precipitation changes projected for the 21st century. *Nat. Commun.* **9**, 1150 (2018).
48. Agel, L. & Barlow, M. How well do CMIP6 historical runs match observed Northeast U.S. precipitation and extreme precipitation-related circulation? *J. Clim.* **33**, 9835–9848 (2020).
49. Karmalkar, A. V., Thibeault, J. M., Bryan, A. M. & Seth, A. Identifying credible and diverse GCMs for regional climate change studies—case study: Northeastern United States. *Clim. Change* **154**, 367–386 (2019).
50. Li, J., Qian, Y., Leung, L. R. & Feng, Z. Summer mean and extreme precipitation over the Mid-Atlantic Region: climatological characteristics and contributions from different precipitation types. *J. Geophys. Res. Atmos.* **126**, e2021JD035045 (2021).
51. Agel, L. et al. Dynamical analysis of extreme precipitation in the US northeast based on large-scale meteorological patterns. *Clim. Dyn.* **52**, 1739–1760 (2019).

52. Chen, M. et al. Assessing objective techniques for gauge-based analyses of global daily precipitation. *J. Geophys. Res.* **113**, D04110 (2008).
53. Sun, Q. et al. A review of global precipitation data sets: data sources, estimation, and intercomparisons. *Rev. Geophys.* **56**, 79–107 (2018).
54. Akinsanola, A. A., Kooperman, G. J., Pendergrass, A. G., Hannah, W. M. & Reed, K. A. Seasonal representation of extreme precipitation indices over the United States in CMIP6 present-day simulations. *Environ. Res. Lett.* **15**, 094003 (2020).
55. Menne, M. J., Durre, I., Vose, R. S., Gleason, B. E. & Houston, T. G. An overview of the Global Historical Climatology Network-Daily database. *J. Atmos. Ocean Tech* **29**, 897–910 (2012).
56. Zhao, M. et al. The GFDL global atmosphere and land model AM4.0/LM4.0: 1. simulation characteristics with prescribed SSTs. *J. Adv. Model Earth Syst.* **10**, 691–734 (2018).
57. Zhao, M. et al. The GFDL global atmosphere and land model AM4.0/LM4.0: 2. model description, sensitivity studies, and tuning strategies. *J. Adv. Model Earth Syst.* **10**, 735–769 (2018).
58. Adcroft, A. et al. The GFDL global ocean and sea ice model OM4.0: model description and simulation features. *J. Adv. Model Earth Syst.* **11**, 3167–3211 (2019).
59. Held, I. M. et al. Structure and performance of GFDL's CM4.0 climate model. *J. Adv. Model Earth Syst.* **11**, 3691–3727 (2019).
60. Dunne, J. P. et al. The GFDL Earth System Model version 4.1 (GFDL-ESM 4.1): overall coupled model description and simulation characteristics. *J. Adv. Model Earth Syst.* **12**, e2019MS002015 (2020).
61. Kriegler, E. et al. Fossil-fueled development (SSP5): an energy and resource intensive scenario for the 21st century. *Glob. Environ. Change* **42**, 297–315 (2017).
62. Riahi, K. et al. The Shared Socioeconomic Pathways and their energy, land use, and greenhouse gas emissions implications: an overview. *Glob. Environ. Change* **42**, 153–168 (2017).
63. Kay, J. E. et al. The Community Earth System Model (CESM) large ensemble project: a community resource for studying climate change in the presence of internal climate variability. *B Am. Meteorol. Soc* **96**, 1333–1349 (2015).
64. AMS. Meteorology glossary. https://glossary.ametsoc.org/wiki/Return_period (2022).
65. Camuffo, D., Becherini, F. & della Valle, A. Relationship between selected percentiles and return periods of extreme events. *Acta Geophys.* **68**, 1201–1211 (2020).

ACKNOWLEDGEMENTS

AUTHOR CONTRIBUTIONS

B.-T.J. and T.L.D. conceived the study. W.F.C. conducted the model simulations. B.-T.J. collected the data and performed the analyses with the help of T.L.D. and K.-C.T. B.-T.J. wrote the first draft of the manuscript. All authors contributed to interpreting the results and provided feedback to improve the manuscript.

COMPETING INTERESTS

The authors declare no competing interests.

ADDITIONAL INFORMATION

Supplementary information The online version contains supplementary material available at https://doi.org/10.1038/s41612-023-00347-w.

Correspondence and requests for materials should be addressed to Bor-Ting Jong.

Reprints and permission information is available at http://www.nature.com/reprints

Publisher's note Springer Nature remains neutral with regard to jurisdictional claims in published maps and institutional affiliations.